Observation of an isotope effect in state-selective mutual neutralization of lithium with hydrogen

Alice F. Schmidt-May [*], Stefan Rosén, MingChao Ji, Gustav Eklund, Henning Zettergren,
Henrik Cederquist, and Henning T. Schmidt [†]
Department of Physics, Stockholm University, Stockholm 10691, Sweden

Paul S. Barklem and Jon Grumer
Theoretical Astrophysics, Department of Physics and Astronomy, Uppsala University, Uppsala 75237, Sweden

We report on mutual neutralization measurements between $^7\text{Li}^+$ and $^1\text{H}^-$ at effective center-of-mass collision energies in the range of 100 to 350 meV. We find that final states of lithium with principal quantum number $n = 3$ dominate with $3s$ separated from the unresolved $3p$ and $3d$ states. We measure the $3s$ branching fraction to be 0.665(12) at 100(16) meV and no significant dependence on collision energy is observed in the studied range. Comparing to previous results on mutual neutralization between $^7\text{Li}^+$ and $^2\text{H}^-$ [G. Eklund *et al.*, Phys. Rev. A **102**, 012823 (2020)], we find that $^7\text{Li}^+$ collisions with $^1\text{H}^-$ result in a significantly higher $3s$ branching fraction than collisions with $^2\text{H}^-$. The difference is 0.087(14). The $3s$ branching fraction of $^7\text{Li}^+ + {}^1\text{H}^-$ and the determined isotope difference are in agreement with results from extended full quantum calculations based on the same input data and numerical method as in Croft *et al.* [H. Croft, A. S. Dickinson, and F. X. Gadéa, J. Phys. B **32**, 81 (1999)]. These calculations reveal strong Stueckelberg oscillations of the $3s$ branching fraction for both isotopes.

I. INTRODUCTION

Hydrogen is the most abundant element in the universe and one of the most important collision partners, especially in the photospheres of cool stars [1–3]. The assumption of local thermodynamic equilibrium is often insufficient for the accurate extraction of elemental abundances from stellar spectra, and thus more sophisticated modeling must be performed, including all of the important radiative and inelastic collisional processes. The significance of mutual neutralization (MN) with hydrogen in such modeling and in general for abundance analyses of cool stars has been demonstrated for the cases of lithium, sodium, and magnesium lines [4–7]. Stellar lithium abundances are of particular interest as they can be used to study stellar evolution and nucleosynthesis, including in the early universe [8–10].

The cross sections that astrophysical models employ to extract elemental abundances stem from calculations for which experimental benchmarking is rare, particularly at the sub-eV collision energies typical of stellar photospheres. At these low collision energies, trajectory effects due to the Coulomb attraction in the initial ion-pair channel become prominent and isotope effects can appear. Despite this, hydrogen is often replaced with deuterium in merged-beams experiments, since smaller mass ratios between the ions in the two beams are generally easier to handle. Experimental data on deuterium are then used to benchmark theoretical results on hydrogen, like in previous MN studies, e.g., for Na^+ with $^2\text{H}^-$ [6,11] and Mg^+ with $^2\text{H}^-$ [12]. It is therefore crucial to investigate the difference between collisions with $^2\text{H}^-$ and with $^1\text{H}^-$.

The influence of a heavier mass on the total and relative partial cross sections is not straightforward to predict. At low collision energies, the calculated total MN cross section is smaller for the heavier isotope in the cases of $\text{H}^+ + \text{Cl}^-$ [13], $\text{Li}^+ + \text{H}^-$, and $\text{Na}^+ + \text{H}^-$ reactions [6], while it is larger in the cases of $\text{H}^+ + \text{H}^-$ [14], $\text{He}^+ + \text{H}^-$ [15], and $\text{H}^+ + \text{F}^-$ [16]. Isotopic changes in the potential-energy curves and in the nonadiabatic-coupling elements are insignificant, as discussed in detail in a recent theoretical study on the isotope effect in MN of $^{1,2}\text{H}^- + {}^{6,7}\text{Li}^+$ [17]. Instead, the mass dependencies of total and relative partial cross sections originate from the change in the radial velocity with which the ions pass avoided crossings of adiabatic potential-energy curves. Isotope effects are predicted by numerous theoretical MN studies [6,13–20]. Yet, to the best of our knowledge, there are no reports on experimental observations of isotope effects in MN prior to the present paper and a parallel independent study of the $\text{He}^+ + \text{H}^-$ system [21].

Earlier, Sawyer *et al.* measured the total MN rate coefficients of $^{1,2}\text{H}^+$ with different halide anions using the flowing-afterglow-Langmuir-probe technique. They observed

*alice.schmidt-may@fysik.su.se
†schmidt@fysik.su.se

no significant difference between ^{1}H$^-$ and ^{2}H$^-$ [22] in contrast to the theoretical predictions [13,16].

Theoretical studies of the MN between ^{7}Li$^+$ and ^{1,2}H$^-$ have been performed with so-called full quantum calculations, quantum chemistry structure calculations in combination with quantum scattering calculations, by Croft *et al.* [19,20]. They used quantum-mechanical scattering dynamics (QS) on empirically improved full configuration-interaction potentials (CI1) of Boutalib and Gadéa [23,24]. However, these calculations were performed only for a handful of collision energies. In this paper, in order to allow a detailed comparison with the experimental results, we have redone these full quantum calculations (CI1-QS) for a more dense and extended grid of collision energies as described in Sec. III C. A study by Belyaev and Voronov used the same *ab initio* potentials by Boutalib and Gadéa with the Landau-Zener (LZ) model and probability current for the dynamics (CI1-LZ) [17]. In a third theoretical investigation by Launoy *et al.*, *ab initio* potentials were calculated via a multireference configuration-interaction approach (CI2) and combined with the multichannel LZ model (CI2-LZ) [18]. A fourth theoretical investigation, by Barklem *et al.*, which we include in our comparison, applied multichannel LZ to potentials from a linear combination of atomic orbitals (LCAO) approach, (LCAO-LZ) [6]. These four theoretical studies of MN of Li$^+$ with ^{1,2}H$^-$ [6,17–20] yield different results on the 3s branching fraction but they all indicate that it is larger for the lighter isotope, ^{1}H$^-$, and that the effect is large enough to be measured with the current capabilities of the DESIREE setup.

Here, we present experimental results on MN between ^{1}H$^-$ and Li$^+$. In combination with a previous study of ^{2}H$^-$ using the same experimental setup at DESIREE [25], we find an isotope effect on the 3s branching fraction in the sub-eV collision energy range and compare the experimental results to the theoretical predictions, including the newly extended full quantum calculations.

II. EXPERIMENT

The present experiment was performed at DESIREE, which is a cryogenic double electrostatic ion-beam-storage-ring facility, which has been described before (see, e.g., Refs. [26,27]). A schematic of the experimental setup is presented in Fig. 1. The lithium cations were produced from lithium bromide in a so-called Nielsen source [28], which is a magnetic ion source with a sublimation furnace attached to the discharge chamber. The hydrogen anions were produced in a source of negative ions by cesium sputtering [29] using TiH$_2$ in a copper cathode. The two ion beams were formed on two different high-voltage platforms and accelerated by potential differences of -7.0 and 45 kV for hydrogen, ^{1}H$^-$, and lithium, ^{7}Li$^+$, ions, respectively. The experimental procedure is described in detail by Eklund *et al.* [25]. In contrast to the experiments with ^{2}H$^-$ described in Ref. [25], the ^{7}Li$^+$ and ^{1}H$^-$ ion beams were not stored for the present experiment, but continuously guided into Faraday cups after the first round trip. This allows for quicker data acquisition but does not change the fundamentals of the experiment for the present collision system in relation to the experiment with deuterium [25].
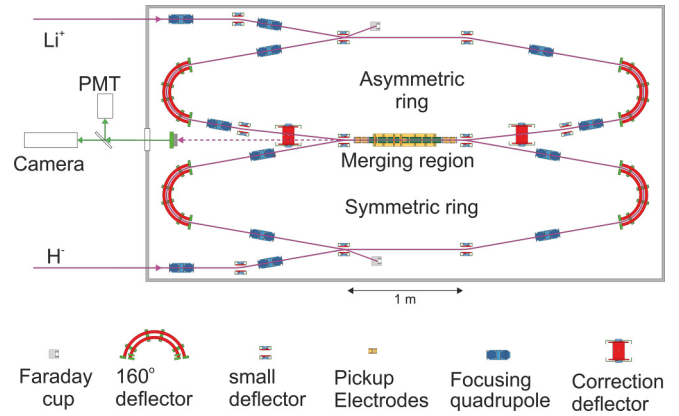

FIG. 1. Schematic depiction of the most relevant parts of DESIREE. The detector is a triple-stack microchannel-plate assembly with a phosphor screen anode. A camera and a segmented photomultiplier tube measure the distances perpendicular and parallel to the ion beams' direction in coincidence. For details see Ref. [25].

The ions are accelerated to slightly different velocities, corresponding to a center-of-mass collision energy of 9.3 eV, and overlapped in the straight merging region. Up to seven drift tubes with a shared, adjustable bias voltage allow the tuning and matching of the beams' velocities. In this way, the center-of-mass collision energies can be reduced and controlled inside the biased drift tubes. The present data were taken at different voltages and with different numbers of biased drift tubes. We refer to an individual experimental setting as one measurement. The branching fraction with the smallest uncertainty stems from a measurement with three drift tubes biased at -472 V. Their combined length is 23.8 cm and the distance between the center of the employed drift tubes and the detector is 176 cm. At the end of the straight merging section, electrostatic deflectors bend the ion beams into their orbits whereas neutrals formed in the merging section continue along straight-line trajectories towards the imaging detector. The detector is a so-called Z stack of three microchannel plates with a phosphor screen anode [30]. The phosphor is observed through vacuum chamber viewports by a CMOS camera and a segmented photomultiplier tube (PMT) as indicated in Fig. 1. This detection setup allows for the simultaneous measurement of arrival time and position. This information is combined as described by Eklund *et al.* to reconstruct a three-dimensional vector, $\vec{r}$, which defines the displacement between the two neutrals when their center of mass passes the detector plane [25]. In spherical polar coordinates, r is the separation of the two neutral products and θ is the polar angle (i.e., the angle between $\vec{r}$ and the normal to the detector plane). The product separation, r, is related to the total kinetic energy, E, after the MN reaction in the center-of-mass system via

$$r = \frac{L}{v}\sqrt{2\frac{E}{\mu}} \tag{1}$$

with v the center-of-mass velocity and μ the reduced mass of the diatomic system. L is the distance from the position of the MN reaction to the detector and its average is equal to

the distance between the center of the biased section and the detector. The total kinetic energy E is the sum of the product-channel-specific kinetic-energy release (KER) of the reaction and the center-of-mass collision energy.

III. ANALYSIS

A. Branching fractions

The two neutrals stemming from a MN reaction in the biased section of the drift tubes arrive only up to tens of nanoseconds apart. The neutral products from a MN reaction outside the biased section, on the other hand, yield two-particle coincidence events with hundreds of nanoseconds higher arrival-time differences due to the unmatched beam velocities in this region. By excluding large arrival-time differences, we can hence separate the coincidence events of the biased section from the ones outside the biased section. Events taking place in the fringe fields, where the electric potential is in transition to the applied bias, cannot be fully discriminated against by this selection. They have higher collision energies than events in the center of the biased section and give rise to tails towards larger values of r. An effective discrimination against these fringe field events was achieved by excluding all events with smaller polar angles, θ. The upper discrimination threshold was individually selected for each measurement compromising between the uncertainty originating from the overlap between the peaks and from the counting statistics. The threshold varied between $\cos\theta = 0.4$ and 0.7 among the different measurements as the overlap and accumulated counts differed. A lower discrimination threshold of $\cos\theta = 0.1$ was introduced to discriminate against small arrival-time differences which cannot be separated from artifacts that occur during the combination of time and position information due to cross-talk between the individual PMT segments. At very low collision energies the $\cos\theta$ distributions of all channels are isotropic and, without a channel-dependent anisotropy, cuts in $\cos\theta$ have no influence on the distribution of r and, hence, no influence on the extracted branching fractions.

We determined the branching into the $3s$ state via binning of the product events. Every event is assigned to a channel when it falls into that channel's specific r range. The resulting branching fraction, F_B, into $3s$ was then obtained as

$$F_B = \frac{n_{3s}}{n_{3s} + n_{3pd}} \qquad (2)$$

with n_{3s} being the accumulated count for the $3s$ channel while n_{3pd} is the corresponding sum of the unresolved $3p$ and $3d$ channels. In Fig. 2, we indicate the channels' r ranges together with their upper and lower limits. The error estimate on the $3s$ branching fraction is based on assuming the most extreme combination of the upper and lower limits. Most of the background signal was removed by the selection in $\cos\theta$. To estimate the potential influence of the remaining background on the branching fraction, we selected a product separation range below the left peak in Fig. 2, and divided the counts present in this selected range by the range's width to obtain the background counts per mm of product separation. The background is then scaled to the
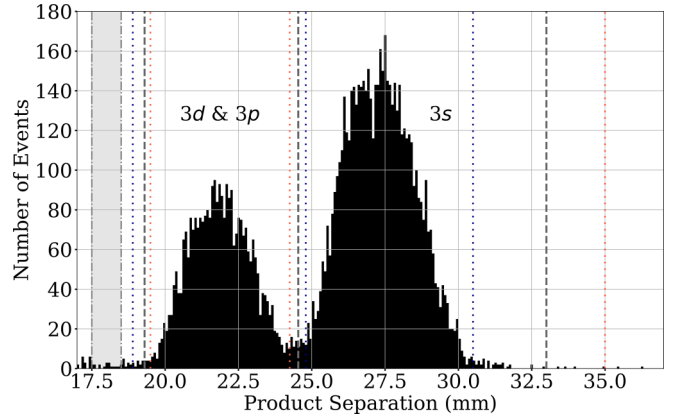

FIG. 2. The distribution of product separations, r, of MN between $^7\text{Li}^+$ with $^1\text{H}^-$ measured with the drift tubes biased at -472 V (later assigned to 100-meV center-of-mass energy). Only events with $0.1 < \cos\theta < 0.4$ are included. The gray, dashed vertical lines mark the boundaries applied for assigning events to the $3s$ channel or the unresolved $3p$ and $3d$ channels. The dotted vertical lines illustrate the uncertainties of these boundaries. Red (lighter gray) dotted lines are combined to create the upper limit of our measured $3s$ F_B and the combination of the blue (darker gray) dotted lines presents the lower limit. The dash-dotted vertical lines, and the shaded area within, define the region of r, which we use to estimate the background.

width of the range for this peak. This background is higher at smaller separations, and the strongest influence on the branching fractions is present if only one spectral feature includes additional random-coincidence events. Consequently, we obtained an error estimate by assuming the background is only present on the low kinetic-energy release channels $3p$ and $3d$, and calculated new branching fractions after subtracting the background. The absolute deviation between the corrected and uncorrected branching fraction was taken as the uncertainty stemming from the background. As the last source of uncertainty for the branching fractions we considered the Poissonian counting statistics. The standard deviations of the counts n_{3s} and n_{3pd} were treated as independent errors and propagated to the branching fractions by applying the variance formula to Eq. (2).

B. Determination of center-of-mass collision energies

We assigned the average center-of-mass collision energy by identifying the energetic shift of the product channels in the energy converted product-separation distribution. The experimental distributions were fitted by three functions with their spacing fixed to the known separation in binding energies for $3s$, $3p$, and $3d$. The functions are convolutions of Gaussians with the kinetic-energy-release distributions expected by the ion-beam velocities modified by the electric potential calculated in SIMION [31]. Following Eklund *et al.* [25], we estimate an uncertainty in the average distance to the detector of 1 cm, and use this uncertainty to obtain the uncertainty in the center-of-mass collision energy. It should be noted that the spread in contributing collision energies is larger than these uncertainties of the average center-of-mass collision energies.

The fitted standard deviation of the convoluted Gaussian can serve as an indication of the spread in collision energies and the fit returns standard deviations of about 70 meV. There are multiple sources causing a spread in center-of-mass energies and a nonzero average. The beams' divergences and velocity spreads are inevitable contributions, and in addition there are contributions from any imperfections in the alignments of the two beams.

C. Full quantum calculations

At low collision energies the most reliable description of atomic collisions is provided by the quantal approach to the dynamics, together with a description of the structure based on molecular orbitals (see, e.g., Refs. [32–34]). As mentioned in the introduction, calculations of this sort were performed for MN in $^7\text{Li}^+ + {}^{1,2}\text{H}^-$ collisions by Croft *et al.* [19,20]. Due to the computational demands of quantum scattering calculations and available computing power at the time, the calculations of Croft *et al.* were performed at only a handful of collision energies and in the case of $^2\text{H}^-$ only at collision energies of 680 meV and higher. In order to allow a detailed comparison with the results at the specific collision energies of the present experiment, we have redone these full quantum calculations for a dense grid of energies, and extending the calculations for $^2\text{H}^-$ to below 680 meV. The calculations are the same as those of Croft *et al.* in terms of the input data used, scattering equations solved, and numerical method employed, but may differ in details such as numerical parameters of the calculations.

Specifically, the scattering theory in the diabatic representation follows that described by Croft *et al.* [19,20] and is solved in practice using the QUANTXS code [35] employing the improved log-derivative method [36,37]. Appropriate asymptotic nuclear wave functions for open channels are used: Ricatti-Bessel functions for the covalent channels, and Coulomb functions for the ionic channel [37–39]. Based on the low collision energies of interest and following the study on $\text{H}^+ + \text{H}^-$ by Fussen and Kubach [40], Croft *et al.* [19,20] did not include electron translation factors (see, e.g., Refs. [41–43]), and the same is true for the extended calculations presented here; ideally, future calculations should include these effects, but our initial purpose here is to extend the existing calculations to include many more values of the collision energy.

The input diabatic potential matrix data are the same as used by Croft *et al.* [19,44] [the matrix **V** in their Eq. (3)]; that is, the original data are from Boutalib and Gadéa [23,24], but an improved ionic potential is used, semiempirically correcting the electron affinity of H (see Fig. 2 of Croft *et al.* [19]). Eight molecular $^1\Sigma^+$ states are treated, including the ionic entrance channel $^7\text{Li}^+ + {}^{1,2}\text{H}^-$ and seven covalent channels dissociating to $\text{Li}(nl) + {}^{1,2}\text{H}$ where $nl = 2s$, $2p$, $3s$, $3p$, $3d$, $4s$, and $4p$. The diabatic potential-energy curves (diagonal elements of the potential matrix **V**) are shown in Fig. 3, where the system of crossings between the ionic and covalent states can be seen.

With the method described above, we performed calculations for the partial cross sections and 3s branching fractions
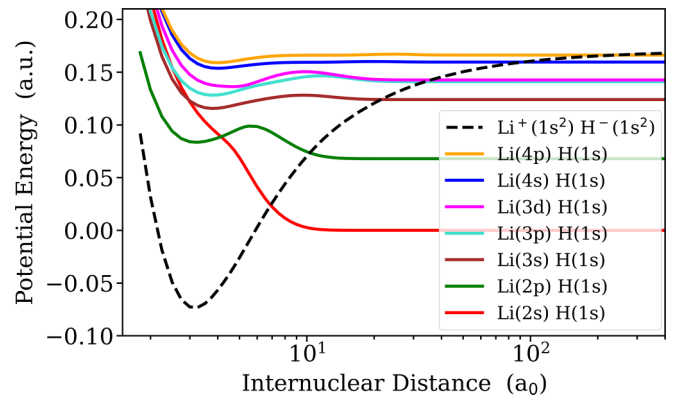

FIG. 3. Diabatic potential-energy curves (diagonal elements of the potential matrix) for LiH as in Croft *et al.* [19] and used in this paper. The potentials are in atomic units and the zero point taken at the asymptotic energy for $\text{Li}(2s) + \text{H}(1s)$. The ionic state, shown as a dashed line, crosses the covalent states, shown as full lines. These crossings provide the mechanism for MN and crossings at moderate internuclear distance (between 20 and 40 a_0) favor the $n = 3$ states.

for $^7\text{Li}^+ + {}^{1,2}\text{H}^-$ on a very fine energy grid with 324 energies between 1 meV and 5 eV. The calculations for the 3s branching fraction agree well with the results derived from Croft *et al.* [19,20] (see Fig. 4); there is a difference of the order of 1% at very low energy for $^7\text{Li}^+ + {}^1\text{H}^-$ that we suspect originates in small differences in the numerical implementation (e.g., parameter choices in the solution of the scattering equations); we have extensively tested that our extended calculations are converged with respect to such parameter choices. The results of the extended calculations presented here show significant structure above 50 meV due to Stueckelberg oscillations in the 3s branching fraction arising from interference effects; see Fig. 4. As the calculations combine CI1 with QS, we refer to them as CI1-QS as already mentioned in the introduction.
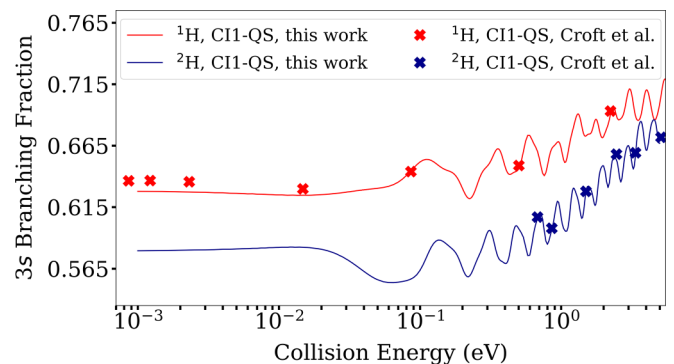

FIG. 4. Calculated 3s branching fractions following MN between $^7\text{Li}^+$ and $^{1,2}\text{H}^-$ as functions of the center-of-mass collision energy with hydrogen in red (lighter gray) and deuterium in blue (darker gray). The data points from the original calculations of Croft *et al.* [19,20] are marked with x and the results of the present extended calculations based on their method for a more dense and extended grid of collision energies are indicated as solid lines.
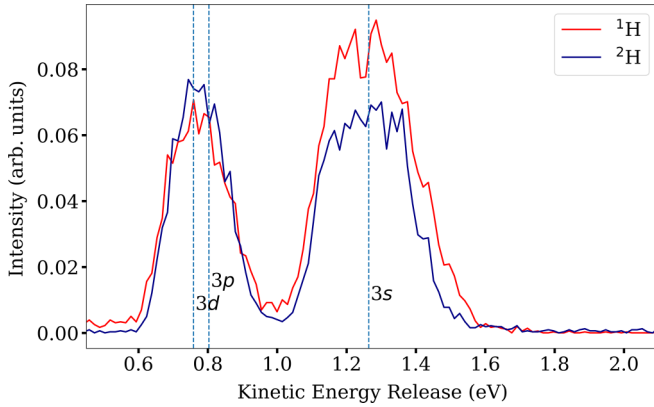
FIG. 5. Measured kinetic-energy-release (KER) distributions of MN between $^7\text{Li}^+$ and hydrogen in red (lighter gray) and deuterium in blue (darker gray). The deuterium data are from a previous study at DESIREE [25]. We used Eq. (1) in combination with the deduced collision energies, which are 100(16) meV for hydrogen and 78(13) meV for deuterium, to convert the measured product separations to KER. Both distributions are normalized to the counts in the unresolved 3p-3d peak.

IV. RESULTS AND DISCUSSION

Our most precise measurement at a center-of-mass collision energy of 100(16) meV yields a branching fraction of 0.665(12) into the 3s state of ^7Li when $^7\text{Li}^+$ neutralizes in collisions with $^1\text{H}^-$. We find no significant change of this ratio with increasing center-of-mass energy up to 350 meV.

The fractional population of the Li(3s) final state in MN collisions between $^7\text{Li}^+$ and $^2\text{H}^-$ has earlier been measured to be 0.578(7) at 78(13) meV [25]. We thus arrive at a difference of 0.087(14) between the results for the $^1\text{H}^-$ and $^2\text{H}^-$ for collision energies close to 100 meV.

In Fig. 5, we display the measured distribution of product separations converted into KER distributions of $^7\text{Li}^+ + {}^1\text{H}^-$ and $^7\text{Li}^+ + {}^2\text{H}^-$, the latter from Eklund *et al.* [25]. The conversion between r and KER is obtained via Eq. (1) and the

respective center-of-mass collision energies are subtracted, so a common E axis is obtained. The distributions are normalized to the integrated counts in the unresolved 3p-3d peak to illustrate the impact on the 3s branching fraction. Despite the small deviations in the peak shapes, which are ascribed to slightly different experimental conditions, the figure illustrates the isotopic dependence of the MN branching fractions.

In Fig. 6, we show a comparison between independent experimental results on the 3s branching fraction at various collision energies and with different hydrogen isotopes and theoretical results from the CI1-QS and LCAO-LZ calculations [6].

In Table I, the present experimental results for $^1\text{H}^-$ and previous experimental results for $^2\text{H}^-$ [25] are shown along with theoretical predictions. Comparing our measured 3s branching fractions for ^1H with the theoretical results, we find agreement with the full quantum calculations, CI1-QS, and with the two studies that combine the LZ model with *ab initio* potentials [17,18]. The LCAO-LZ approach slightly overestimates the 3s branching fraction.

The observed isotope difference of 0.087(14) agrees only with the difference predicted by the full quantum calculations. All other theoretical results predict that the 3s fraction is higher for $^1\text{H}^-$ than for $^2\text{H}^-$ in agreement with the experimental result, but underestimate the difference by up to about a factor of 2. We would like to point out that the level of agreement with the CI1-QS depends on the position of minima and maxima of the pronounced Stueckelberg oscillations in these full quantum results. The exact position of the oscillations is very likely sensitive to the finer details of the potentials; see for example Fig. 7 of Ref. [45]. The uncertainties in our experimental results, including the spread of contributing collision energies, do not allow specific conclusions about the details of the oscillations.

The observation of an increase of the branching fraction into a lower excited state, in our case 3s, when the lighter isotope is used, agrees with the trend based on an approximate, asymptotic theoretical model introduced and discussed by Dochain *et al.* [21].
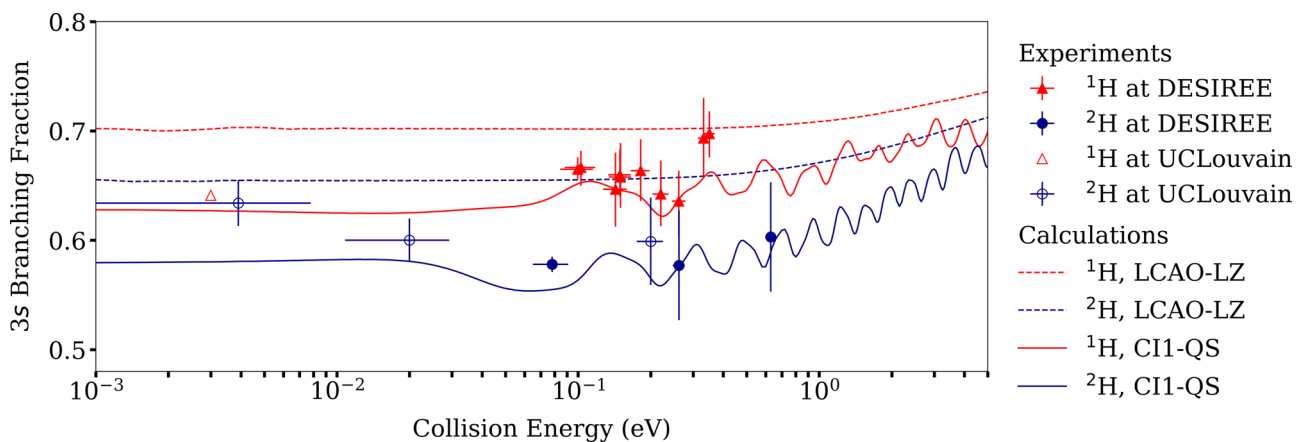

FIG. 6. Branching fractions into the 3s state of lithium in MN of $^7\text{Li}^+$ and $^{1,2}\text{H}^-$ at different collision energies for hydrogen (red, or lighter gray) and deuterium (blue, or darker gray). The theoretical results displayed here are the present CI1-QS calculations (see Sec. III C) shown as solid lines and the LCAO-LZ calculations by Barklem *et al.* [6] shown as dashed lines. The experimental data points include, besides the present results, a previous study at DESIREE of $^2\text{H}^-$ [25] and corresponding results, mainly on $^2\text{H}^-$ of Launoy *et al.* [18] labeled with their affiliation Université Catholique de Louvain. Note the logarithmic x axis.

TABLE I. Comparison between the measured $^7\text{Li}^+ + {}^1\text{H}^-/{}^2\text{H}^- \rightarrow {}^7\text{Li}^{+*}(nl) + {}^1\text{H}/{}^2\text{H}$ branching fractions for state-specific mutual neutralization, and the resulting isotopic difference, with available calculations using different theoretical approaches. The experimental $3s$ branching fractions were measured at a collision energy of 100(16) and 78(13) meV for ^1H and ^2H, respectively. ^2H results stem from Ref. [25]. The theoretical QC-LZ(PC) [17], LCAO-LZ [6], and CI1-QS values are interpolated to the respective energy. The tabulated branching fractions of the CI1-LZ(PC) [17] and CI2-LZ [18] stem from rate coefficients. The rate coefficients were tabulated at 2000 and 1000 K in the case of CI2-LZ and CI1-LZ(PC), respectively.

	Measured	CI1-QS	CI1-LZ(PC)	CI2-LZ	LCAO-LZ
$^1\text{H} + \text{Li}(3s)$	0.665(12)	0.652	0.660	0.667	0.702
$^2\text{H} + \text{Li}(3s)$	0.578(7)	0.555	0.593	0.608	0.656
Isotopic difference	0.087(14)	0.097	0.067	0.059	0.046

V. CONCLUSIONS

We present experimental results on the branching fraction into lithium's $3s$ state in $^7\text{Li}^+ + {}^1\text{H}^-$ reactions for collision energies between 100 and 350 meV and compare them with the corresponding earlier results from Ref. [25] for $^2\text{H}^-$. For $^1\text{H}^-$, we measured the $3s$ branching fraction to be 0.665(12) at an average collision energy of 100(16) meV and found no significant dependence of the $3s$ branching fraction on the collision energy in the studied energy range. This experimental $3s$ branching fraction agrees with the results of the full quantum calculations and of the theoretical studies combining *ab initio* potentials with Landau-Zener dynamics. In combination with the previous MN study between $^7\text{Li}^+$ and $^2\text{H}^-$ [25], also performed at DESIREE, we report a significant isotopic difference of 0.087(14) in the $3s$ branching fraction. This is consistent with the isotope effect predicted by full quantum calculations but deviates by about a factor of 2 from the predictions of the LCAO approach. In addition, full quantum calculation results predict strong Stueckelberg oscillations of the $3s$ branching fractions for both isotopes with a significant influence on the energy dependence of the isotopic difference in the $3s$ branching fraction.

All resulting data shown in the figures are available electronically under a Creative Commons license [46].

[1] W. Steenbock and H. Holweger, Statistical equilibrium of lithium in cool stars of different metallicity, Astron. Astrophys. **130**, 319 (1984).

[2] P. S. Barklem, A. K. Belyaev, M. Guitou, N. Feautrier, F. X. Gadéa, and A. Spielfiedel, On inelastic hydrogen atom collisions in stellar atmospheres, Astron. Astrophys. **530**, A94 (2011).

[3] L. Mashonkina, Atomic data necessary for the non-LTE analysis of stellar spectra, Phys. Scr. **T134**, 014004 (2009).

[4] P. S. Barklem, A. K. Belyaev, and M. Asplund, Inelastic H + Li and H$^-$ + Li$^+$ collisions and non-LTE Li i line formation in stellar atmospheres, Astron. Astrophys. **409**, L1 (2003).

[5] K. Lind, M. Asplund, and P. S. Barklem, Departures from LTE for neutral Li in late-type stars, Astron. Astrophys. **503**, 541 (2009).

[6] P. S. Barklem, A. M. Amarsi, J. Grumer, G. Eklund, S. Rosén, M. C. Ji, H. Cederquist, H. Zettergren, and H. T. Schmidt, Mutual neutralization in Li$^+$ + H$^-$/D$^-$ and Na$^+$ + H$^-$/D$^-$ collisions: Implications of experimental results for non-LTE modeling of stellar spectra, Astrophys. J. **908**, 245 (2021).

[7] Y. Osorio, P. S. Barklem, K. Lind, A. K. Belyaev, A. Spielfiedel, M. Guitou, and N. Feautrier, Mg line formation in late-type stellar atmospheres. I. The model atom, Astron. Astrophys. **579**, A53 (2015).

[8] A. J. Korn, F. Grundahl, O. Richard, P. S. Barklem, L. Mashonkina, R. Collet, N. Piskunov, and B. Gustafsson, A probable stellar solution to the cosmological lithium discrepancy, Nature (London) **442**, 657 (2006).

[9] J. C. Howk, N. Lehner, B. D. Fields, and G. J. Mathews, Observation of interstellar lithium in the low-metallicity small magellanic cloud, Nature (London) **489**, 121 (2012).

[10] E. X. Wang, T. Nordlander, M. Asplund, A. M. Amarsi, K. Lind, and Y. Zhou, 3D NLTE spectral line formation of lithium in late-type stars, Mon. Not. R. Astron. Soc. **500**, 2159 (2020).

[11] G. Eklund, J. Grumer, P. S. Barklem, S. Rosén, M. C. Ji, A. Simonsson, R. D. Thomas, H. Cederquist, H. Zettergren, and H. T. Schmidt, Final-state-resolved mutual neutralization of Na$^+$ and D$^-$, Phys. Rev. A **103**, 032814 (2021).

[12] J. Grumer, G. Eklund, A. M. Amarsi, P. S. Barklem, S. Rosén, M. C. Ji, A. Simonsson, H. Cederquist, H. Zettergren, and H. T. Schmidt, State-resolved mutual neutralization of Mg$^+$ and D$^-$, Phys. Rev. Lett. **128**, 033401 (2022).

[13] Å. Larson, J. Hörnquist, P. Hedvall, and A. E. Orel, Mutual neutralization in collisions of $H^+ + Cl^-$, J. Chem. Phys. **151**, 214305 (2019).

[14] S. M. Nkambule, N. Elander, Å. Larson, J. Lecointre, and X. Urbain, Differential and total cross sections of mutual neutralization in low-energy collisions of isotopes of $H^+ + H^-$, Phys. Rev. A **93**, 032701 (2016).

[15] Å. Larson, S. M. Nkambule, and A. E. Orel, Theoretical study of mutual neutralization in $He^+ + H^-$ collisions, Phys. Rev. A **94**, 022709 (2016).

[16] J. Z. Mezei, J. B. Roos, K. Shilyaeva, N. Elander, and Å. Larson, Mutual neutralization in low-energy $H^+ + F^-$ collisions, Phys. Rev. A **84**, 012703 (2011).

[17] A. K. Belyaev and Y. V. Voronov, Isotopic effects in low-energy lithium-hydrogen collisions, Phys. Rev. A **104**, 022812 (2021).

[18] T. Launoy, J. Loreau, A. Dochain, J. Liévin, N. Vaeck, and X. Urbain, Mutual neutralization in $Li^+ + H^-$ collisions: A combined experimental and theoretical study, Astrophys. J. **883**, 85 (2019).

[19] H. Croft, A. S. Dickinson, and F. X. Gadéa, A theoretical study of mutual neutralization in in $Li^+ + H^-$ collisions, J. Phys. B **32**, 81 (1999).

[20] H. Croft, A. S. Dickinson, and F. X. Gadéa, Rate coefficients for the Li^+/H^- and Li^-/H^+ mutual neutralization reactions, Mon. Not. R. Astron. Soc. **304**, 327 (1999).

[21] A. Dochain, V. M. Andrianarijaona, and X. Urbain, companion paper, Isotope effect for the mutual neutralization reaction at low collision energies: $He^+ + H^-$, Phys. Rev. A **108**, 042809 (2023).

[22] J. C. Sawyer, T. M. Miller, B. C. Sweeny, S. G. Ard, A. A. Viggiano, and N. S. Shuman, Mutual neutralization of H^+ and D^+ with the atomic halide anions Cl^-, Br^-, and I^-, J. Chem. Phys. **149**, 044303 (2018).

[23] A. Boutalib and F. X. Gadéa, Ab initio adiabatic and diabatic potential-energy curves of the LiH molecule, J. Chem. Phys. **97**, 1144 (1992).

[24] F. X. Gadéa and A. Boutalib, Computation and assignment of radial couplings using accurate diabatic data for the LiH molecule, J. Phys. B **26**, 61 (1993).

[25] G. Eklund, J. Grumer, S. Rosén, M. C. Ji, N. Punnakayathil, A. Källberg, A. Simonsson, R. D. Thomas, M. H. Stockett, P. Reinhed, P. Löfgren, M. Björkhage, M. Blom, P. S. Barklem, H. Cederquist, H. Zettergren, and H. T. Schmidt, Cryogenic merged-ion-beam experiments in DESIREE: Final-state-resolved mutual neutralization of Li^+ and D^-, Phys. Rev. A **102**, 012823 (2020).

[26] R. D. Thomas, H. T. Schmidt, G. Andler, M. Björkhage, M. Blom, L. Brännholm, E. Bäckström, H. Danared, S. Das, N. Haag, P. Halldén, F. Hellberg, A. I. S. Holm, H. A. B. Johansson, A. Källberg, G. Källersjö, M. Larsson, S. Leontein, L. Liljeby, P. Löfgren *et al.*, The double electrostatic ion ring experiment: A unique cryogenic electrostatic storage ring for merged ion-beams studies, Rev. Sci. Instrum. **82**, 065112 (2011).

[27] H. T. Schmidt, R. D. Thomas, M. Gatchell, S. Rosén, P. Reinhed, P. Löfgren, L. Brännholm, M. Blom, M. Björkhage, E. Bäckström, J. D. Alexander, S. Leontein, D. Hanstorp, H. Zettergren, L. Liljeby, A. Källberg, A. Simonsson, F. Hellberg, S. Mannervik, M. Larsson *et al.*, First storage of ion beams in the double electrostatic ion-ring experiment: Desiree, Rev. Sci. Instrum. **84**, 055115 (2013).

[28] K. O. Nielsen, The development of magnetic ion sources for an electromagnetic isotope separator, Nucl. Instrum. **1**, 289 (1957).

[29] National Electrostatics Corp., Source of negative ions by cesium sputtering—SNICSII, https://www.pelletron.com/wp-content/uploads/2017/02/SNICS-v2.pdf (2017).

[30] S. Rosén, H. T. Schmidt, P. Reinhed, D. Fischer, R. D. Thomas, H. Cederquist, L. Liljeby, L. Bagge, S. Leontein, and M. Blom, Operating a triple stack microchannel plate-phosphor assembly for single particle counting in the 12–300K temperature range, Rev. Sci. Instrum. **78**, 113301 (2007).

[31] Dahl, D A., Simion 3D version 6.0, User's Manual. United States: N. p., 1995. Web. doi: 10.2172/130674.

[32] A. Macías and A. Riera, Ab initio quantum chemistry in the molecular model of atomic collisions, Phys. Rep. **90**, 299 (1982).

[33] M. Kimura and N. F. Lane, The low-energy, heavy-particle collisions: A close-coupling treatment, in *Advances in Atomic, Molecular, and Optical Physics*, edited by S. D. Bates and B. Bederson (Academic Press, New York, 1989), Vol. 26, pp. 79–160.

[34] B. H. Bransden, M. R. C. McDowell, B. H. Bransden, and M. R. C. McDowell, *Charge Exchange and the Theory of Ion-Atom Collisions*, International Series of Monographs on Physics (Oxford University Press, New York, 1992).

[35] R. J. Allan, Atomic physics on high-performance (parallel) computers, in *New Directions in Atomic Physics*, edited by C. T. Whelan, R. M. Dreizler, J. H. Macek, and H. R. J. Walters (Springer, New York, 1999), pp. 281–290.

[36] D. E. Manolopoulos, An improved log derivative method for inelastic scattering, J. Chem. Phys. **85**, 6425 (1986).

[37] B. R. Johnson, The multichannel log-derivative method for scattering calculations, J. Comput. Phys. **13**, 445 (1973).

[38] A. R. Barnett, COULFG: Coulomb and Bessel functions and their derivatives, for real arguments, by Steed's method, Comput. Phys. Commun. **27**, 147 (1982).

[39] A. R. Barnett, The calculation of spherical Bessel and Coulomb functions, in *Computational Atomic Physics: Electron and Positron Collisions with Atoms and Ions*, edited by K. Bartschat (Springer-Verlag, Berlin, 1996), pp. 181–202.

[40] D. Fussen and C. Kubach, Theoretical study of mutual neutralisation in H^+-H^- collisions at low energy (0.02–20 eV), J. Phys. B **19**, L31 (1986).

[41] D. R. Bates and R. McCarroll, Electron capture in slow collisions, Proc. R. Soc. A **245**, 175 (1958).

[42] L. F. Errea, L. Mendez, and A. Riera, On the choice of translation factors for approximate molecular wavefunctions, J. Phys. B **15**, 101 (1982).

[43] J. Grosser, T. Menzel, and A. K. Belyaev, Approach to electron translation in low-energy atomic collisions, Phys. Rev. A **59**, 1309 (1999).

[44] A. Dickinson and X. Gadéa (private communication).

[45] A. K. Belyaev, P. S. Barklem, A. S. Dickinson, and F. X. Gadéa, Cross sections for low-energy inelastic $H + Na$ collisions, Phys. Rev. A **81**, 032706 (2010).

[46] The data are available at the following repository: http://dx.doi.org/10.5281/zenodo.8273007.